

Rapid Discovery of a Novel Series of Abl Kinase Inhibitors by Application of an Integrated Microfluidic Synthesis and Screening Platform

Bimbisar Desai,[†] Karen Dixon,[†] Elizabeth Farrant,[†] Qixing Feng,[†] Karl R. Gibson,[‡] Willem P. van Hoorn,[§] James Mills,[‡] Trevor Morgan,[†] David M. Parry,[†] Manoj K. Ramjee,[†] Christopher N. Selway,^{*,†} Gary J. Tarver,[†] Gavin Whitlock,[‡] and Adrian G. Wright[†]

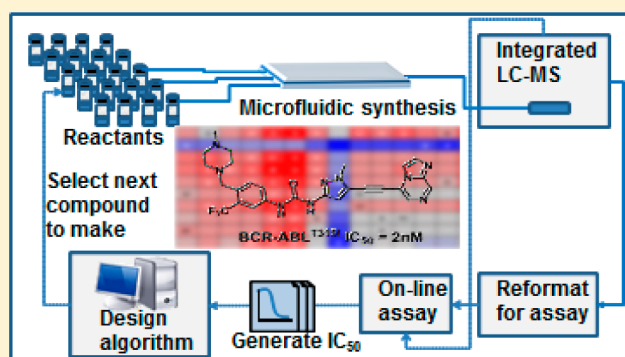
[†]Cyclofluidic Ltd, Biopark, Broadwater Road, Welwyn Garden City, AL7 3AX, U.K.

[‡]Sandexis LLP, Discovery Park, Sandwich, Kent CT13 9ND, U.K.

[§]Accelrys Ltd, 334 Cambridge Science Park, Cambridge, CB4 0WN, U.K.

S Supporting Information

ABSTRACT: Drug discovery faces economic and scientific imperatives to deliver lead molecules rapidly and efficiently. Using traditional paradigms the molecular design, synthesis, and screening loops enforce a significant time delay leading to inefficient use of data in the iterative molecular design process. Here, we report the application of a flow technology platform integrating the key elements of structure–activity relationship (SAR) generation to the discovery of novel Abl kinase inhibitors. The platform utilizes flow chemistry for rapid in-line synthesis, automated purification, and analysis coupled with bioassay. The combination of activity prediction using Random-Forest regression with chemical space sampling algorithms allows the construction of an activity model that refines itself after every iteration of synthesis and biological result. Within just 21 compounds, the automated process identified a novel template and hinge binding motif with $pIC_{50} > 8$ against Abl kinase — both wild type and clinically relevant mutants. Integrated microfluidic synthesis and screening coupled with machine learning design have the potential to greatly reduce the time and cost of drug discovery within the hit-to-lead and lead optimization phases.



1. GENERAL INTRODUCTION

The process of discovering a drug (Figure 1) is slow and expensive, with the average cost of developing a new molecular entity (NME) now estimated at \$1.8 billion.¹

Recent analysis¹ has shown that for every NME launched, 19.4 hit-to-lead programs are required at a cost per launch of \$166 million, due to the high attrition rates in the drug discovery process. Although much of this attrition (27%) is attributed to lack of efficacy in humans in phase II, the majority is reported to be related to problems of safety, toxicology, formulation, pharmacokinetics, and cost of goods (53%).² These characteristics are defined by the chemical structure of the molecule itself.

Drug structures have been shown^{3–5} to be very closely related to their lead compound series and these lead series to the hit series from which they were optimized, indicating that much of the success or failure of a potential drug molecule is laid down at this very early point in the drug discovery process. The decision regarding which lead series to pursue in the hit-to-lead phase is therefore crucial and often dictates the success or

otherwise of the program as well as the time and resources required to launch.

Small molecule lead discovery involves an iterative process of molecular design, chemical synthesis, biological assay, and data analysis to feed into the next learning cycle. In a typical hit-to-lead project, *in vitro* assays are used to measure the potency and selectivity of the molecule at the target of interest as well as a range of calculated and measured physical properties that help to predict a lead molecule's "drug-likeness".^{4,6,7} Using conventional approaches, each learning cycle in this process takes 1–8 weeks, depending on where compounds are made and tested. These cycle times lead to slow and expensive hit-to-lead exploration, limiting the number of lead series that can be assessed. One of the key bottle-necks in this iterative process is the time taken in synthesis and screening activities, which lengthens the time between hypothesis generation/compound design and the result (test data) of that design. This has two potential detrimental effects to a drug discovery program,

Received: January 21, 2013

Published: February 26, 2013

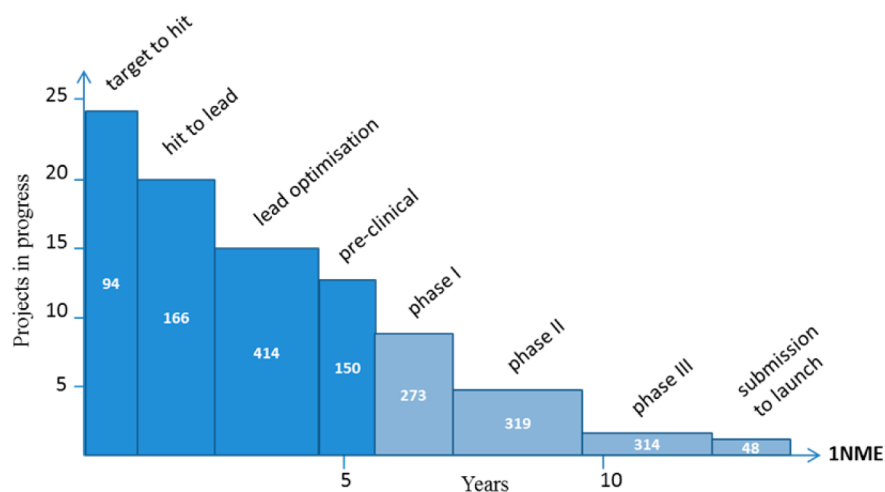


Figure 1. Drug discovery pipeline to produce one NME including cost per phase (\$M).

either: (1) low program velocity — the number of design loops undertaken in a given time frame may be limited, reducing the progress that can be made; or (2) design “at risk” — designs are made without full integration of the test results into the hypothesis generation and design because the assay result of the previous iteration is often not yet available when the next design iteration occurs. Both of these factors, separately or in combination, reduce program productivity.

To accelerate hit-to-lead processes, design hypotheses can be explored in parallel. For example, if orthogonal stripes of analogues are made from within a virtual matrix this allows more rapid mapping of chemical space. Structure–activity relationship (SAR) analysis can then be used to predict where the most active compounds lie (Figure 2). This approach is

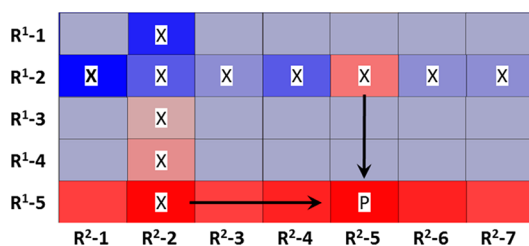


Figure 2. Synthesis of two stripes of analogues (shown with an X) within a matrix can be used to predict active compounds (e.g., P) if SAR is additive.

most effective in those cases where SAR is additive; i.e., in the case shown in Figure 2, the two axes represent independent structural changes in which one structural change does not interact or effect the activity of a structural change on the other axis.^{8,9} However, the rate-limiting steps of synthesis and screening still reduce the efficiency of this process, and the matrix of active compounds will be poorly understood and predicted in cases where SAR is nonadditive.¹⁰

In this paper, we detail a practical example of integrated hit-to-lead optimization using a microfluidic synthesis and screening approach^{11–13} (Figure 3), coupled with a “design layer” activity mapping algorithm facilitating sampling within multidimensional chemical space, thereby creating a bioactivity prediction model that is automatically updated after every single screening result. For the work described here, “virtual chemical space” is defined as the set of molecules that the

prediction model can select from and that *could* be synthesized during an automated experiment — the set is defined by a combination of the microfluidic chemical reactions and the diversity of reactants available on the automated system. Some chemistry development time is required to ensure that analogues can be made in a microfluidic reactor, and the efficient resolution of synthetic chemistry challenges is critical to the success of this approach. To assist this there is an expanding repertoire of flow chemistry reactions appearing in the literature.^{14–20} The automated “in line” nature of microfluidic synthesis, purification, and screening means that a “continuous design process” is possible, with the objective of accurately mapping the SAR within the virtual chemical space using as few design–synthesis–screening loops as possible.

Initially, this approach mirrors that of a traditional hit-to-lead program, namely, hit generation activities via, for example, high-throughput screening (HTS), other screening approaches, or prior art review. From this, the virtual chemical space of target molecules is constructed that defines the boundaries of an SAR heat map. An initial activity model is then built using data available from a screening campaign or the literature against the defined biological target. This model is used to decide which analogue is made during each iteration of synthesis and testing, and the model is updated after each individual compound assay to incorporate the new data. Typically the coupled design, synthesis, and assay times are 1–2 h per iteration.

Two design strategies are used to efficiently explore the virtual chemical space. The initial activity model undergoes an intensive learning process by systematically sampling unknown areas of the space — “most active under sampled”. For 20 design–synthesis–screening runs, this could be completed within 24 h. Depending on the preferences set the next step of iterative design is guided by this updated activity model. For example, further iterations can then be carried out to “chase potency” and rapidly identify the most active compounds in the virtual chemical space, while still only making a small percentage of the molecules within that space. The aim is to map out biological activity for the series by making a small number of compounds, quickly identifying areas of potent and weak activity without having to make large numbers of compounds. These two strategies are complementary when applied within a particular project, allowing both exploration of new reagents and the optimization of activity.

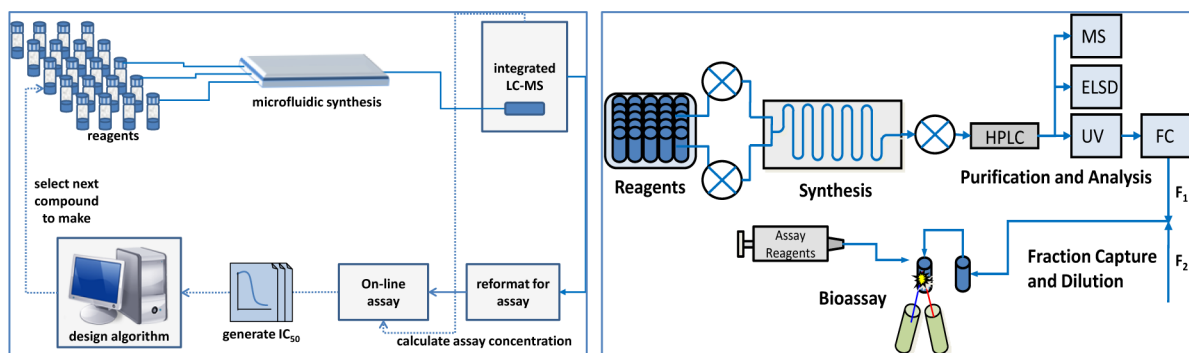


Figure 3. (Left) Schematic of the integrated design, synthesis, and screening platform illustrating the fully automated processes implemented for closed-loop drug discovery. Following initiation of the process the system completes multiple iterations of design, synthesis, and screening without manual intervention. (Right) Schematic showing the continuous fluidic path taken by reagents and products on the platform. A full description of the platform is provided in the Supporting Information.

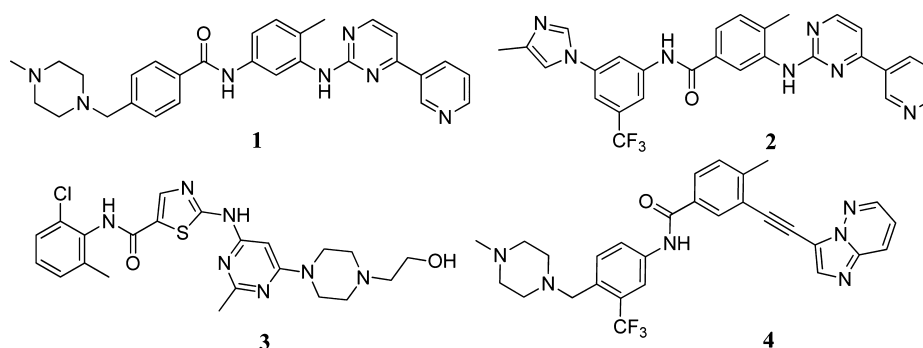


Figure 4. First, second, and third generation BCR-Abl kinase inhibitors.

The potential of this technology is illustrated here through its application to the discovery of novel breakpoint cluster region Abelson tyrosine kinase (BCR-Abl) inhibitors.

The discovery of BCR-Abl inhibitors (Figure 4) has revolutionized the treatment of chronic myeloid leukemia (CML). The first BCR-Abl inhibitor to be launched, imatinib (**1**), shows robust clinical efficacy and is now a front-line therapy for the treatment of CML.²¹ However, a small number of patients on imatinib therapy relapse and become imatinib-resistant.²² Second generation inhibitors nilotinib (**2**)²³ and dasatinib (**3**)²⁴ have shown efficacy against several clinically relevant mutations in the Abl active site. However, imatinib, nilotinib, and dasatinib all show poor activity against the T315I “gatekeeper” mutant, which is responsible for around 15–20% of all clinical mutants.²⁵ The third generation BCR-Abl inhibitor ponatinib (**4**)²⁶ has shown impressive clinical efficacy in patients expressing the T315I mutation²⁷ and has recently been approved by the FDA.²⁸ The ability of a number of Abl kinase mutations to confer resistance against the first and second generation agents means that BCR-Abl remains an attractive drug target that warrants continued investigation.²⁹

BCR-Abl thus provides a clinically relevant drug target to demonstrate all aspects of the integrated microfluidic synthesis–screening approach (virtual chemical space enumeration, design layer algorithms, automated synthesis–screening–design loops). The significant existing knowledge around the target also enables an assessment of whether this approach could quickly find novel inhibitors in an area with significant prior art and demonstrate whether the methodology can rapidly deliver successful hit-to-lead optimization against soluble protein targets such as kinases. Finally, validated bioassays³⁰

and commercially available reagents³¹ would minimize assay development time. All compounds prepared would be tested at both Abl1 and Abl2 kinase subtypes, although activity models and compound selection would be on the basis solely of Abl1 kinase activity.

2. PROJECT SETUP

2.1. Defining the Virtual Chemical Space. A thorough review of the Abl inhibitor prior art was undertaken to assess the templates from which to define a relevant virtual chemical space. The focus was primarily on those templates that had shown the potential to inhibit the T315I mutant enzyme. The alkyne series exemplified by ponatinib combines wild type (WT) Abl inhibition along with potent activity at key mutants such as T315I.²⁶ An X-ray structure of ponatinib bound to Abl kinase has been published and the binding mode is understood.³² The series contains an imidazopyridazine hinge binding group linked to a structural motif that binds to the “DFG out” conformation of Abl and terminates in a pendant basic amine. The alkyne series also offer some synthetic advantages, giving the potential to build a matrix of hinge-binding heterocycles and a series of alternative DFG-out binding units, while performing the key carbon–carbon bond forming reaction under flow chemistry conditions (Figure 5).

A key criterion for operating in this template was delivering a new series of Abl inhibitors, and we reasoned that novelty could come both from previously unexplored hinge-binding heterocycles and potential DFG-binding motifs. The search for such motifs focused on identifying structures that would occupy the DFG out conformation and also present an acetylene linker at the correct vector to deliver the hinge binding group.

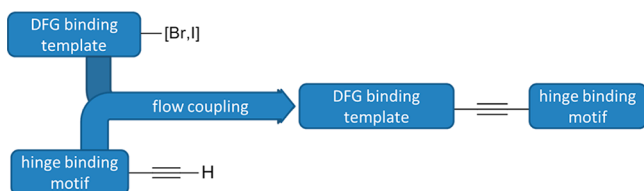


Figure 5. Design of the virtual chemical space for acetylene-linked Abl inhibitors.

A protein data bank (PDB)³⁴ mining approach was used to identify potential alternative core groups that express vectors similar to those present in ponatinib in its binding conformation, as observed in PDB entry 3OXZ (Figure 6). An in-house database of all ligands observed in the PDB was mined to identify all pairs of acyclic single bonds that match these two vectors to within a 0.5 Å threshold. These results were filtered by overlapping the resultant linker moieties into the 3OXZ crystal structure and removing those that clearly gave steric clashes. The remaining examples were assessed by eye, prioritizing those that could retain the hydrogen-bonding features present in the original ligand, or modifying them slightly to accommodate these interactions. Of the groups that emerged from this analysis three were selected and are shown in Figure 7. The amide template **A**, to which ponatinib belongs, was included to determine if novel heterocycle hinge binding motifs could quickly be found in this experiment. Whereas there was some precedence for the reversed amide template **B**,³⁵ the pyrazole urea **C** was an unprecedented replacement in Abl, and would represent a clearly novel inhibitor series if found to be active.

On the basis of precedented synthetic methods,³⁶ we rationalized that Sonogashira coupling of the DFG template halides with a set of aryl/heteroaryl alkynes (Figure 8) would allow the hinge binding heterocycle R^2 to be incorporated in the integrated synthesis–screening flow apparatus.

Relatively few heteroaryl alkynes are commercially available, but around 1000 of their precursor bromo- or iodo-heterocycles are available.³⁷ This large number of potential R^2 groups was triaged by examining the nature of other hinge binding motifs as observed in other kinase PDB crystal structures. To achieve this, a BLAST search of the in-house PDB ligand database was conducted yielding 705 entries with a ligand bound to a protein with high sequence similarity to Abl. All of these PDB binding sites were overlaid onto that of 3OXZ using a quaternion method,³⁸ implemented using the Tinker molecular modeling software suite,³⁹ to overlap the binding site backbone atoms. The resultant overlaps were then filtered to those in which there is a bond that overlays with the bond joining the core to

R^2 (RMS < 0.2 Å). The moieties showing some overlap with the imidazopyridazine group of ponatinib were considered as potential Abl R^2 groups if they were able to mimic the hydrogen-bonding functionality of the ponatinib imidazopyridazine (i.e., the hydrogen bonds to E316O, M318N, and M318O). The most commonly observed R^2 substructure to meet these criteria was a heterocycle with a nitrogen acceptor atom in the 3-position relative to the core attachment point (Figure 9). Therefore, a diverse selection of 27 such R^2 groups was made from the list of bromoheterocycles, including a control selection of building blocks (R^2 = substituted phenyl) that were expected not to bind but could serve to test the ability of the model to discriminate inactives.

As R^2 was the main area targeted for diversity in the virtual chemical space, only a small range of R^1 basic groups was chosen, some with precedent from the Abl literature, and others that had not been exemplified before, such as 4-hydroxypiperidine (Figure 10).

2.2. Chemistry. Template Synthesis. A total of 10 DFG binding templates (Table 1) were synthesized using the synthetic schemes outlined below, which are separated into three chemical series.

Ponatinib templates **A** to generate direct analogues of ponatinib were synthesized according to Scheme 1. An S_N2 substitution of 2-trifluoromethyl-4-nitro benzyl bromide **5**⁴⁰ was carried out with amines **9–12**. Reduction of the aryl nitro intermediates **6** to the corresponding anilines **7** was achieved using Raney Nickel (CatCart) catalyzed hydrogenation in a H-Cube hydrogenation reactor.⁴¹ Finally, the four iodobenzamide templates **8-1** to **8-4** were prepared by reaction of anilines **7** with 3-iodo-4-methylbenzoyl chloride (prepared by refluxing 3-iodo-4-methylbenzoic acid in thionyl chloride). In addition, the un-substituted aniline derivative **8-5** was prepared by reaction of 3-iodo-4-methylbenzoyl chloride with aniline.

The reversed amide templates **B** were prepared according to Scheme 2. Bromination of the acid **13** was achieved using sodium bromate and sodium hydrogen sulfite⁴² and cleanly gave the intermediate bromoacid **14** which was coupled with 3-iodo-4-methyl aniline using 1-chloro-*N,N*,2-trimethyl-1-propenylamine to give intermediate **15**. Subsequent displacement reactions with amines **9–12** and standard purification methods gave the four required templates **16-1** to **16-4**.

The pyrazole urea based template **C** was prepared according to Scheme 3. Piperazine **17** formed from reaction of compound **5** with **9** and subsequent H-Cube reduction was treated with carbonyl diimidazole in DMSO for 30 min and subsequently treated with aminopyrazole **18** for 1 h at room temperature. Standard purification methods furnished the bromopyrazole **19**.

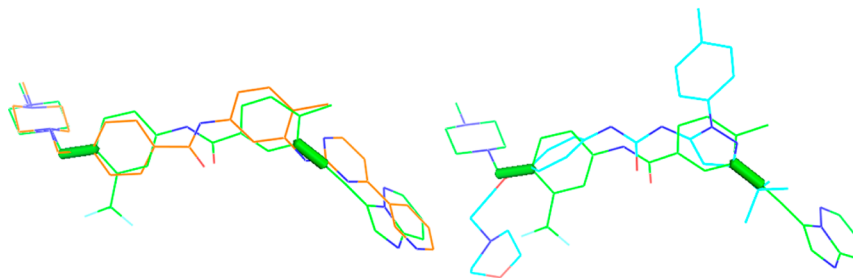


Figure 6. Superposition of two molecules that mimic the linker bonds of ponatinib (green) as observed in its Abl-binding conformation (PDB entry 3OXZ). The reverse amide (orange) is found in a ligand bound to ABL2 (3GVU) and the pyrazole (cyan) in a p38-binding ligand (3HV6).³³

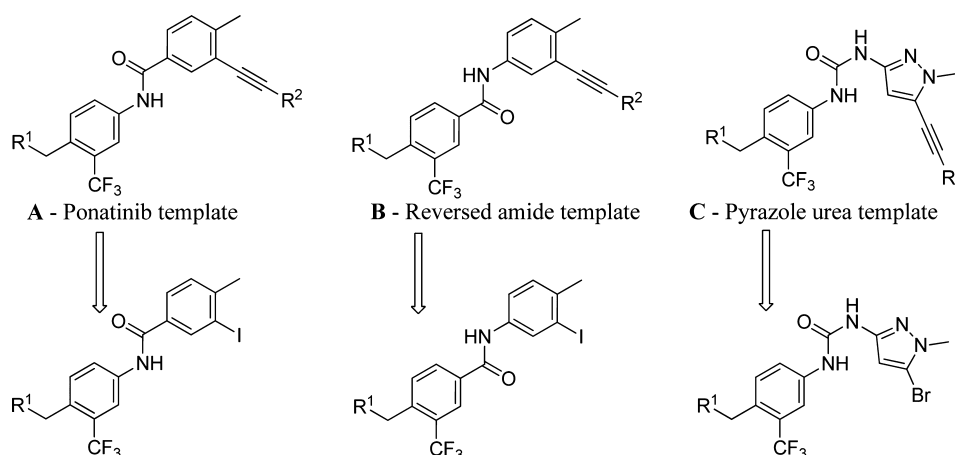


Figure 7. Selected DFG binding templates for virtual chemical space construction and their synthetic precursors used in the experimental work.

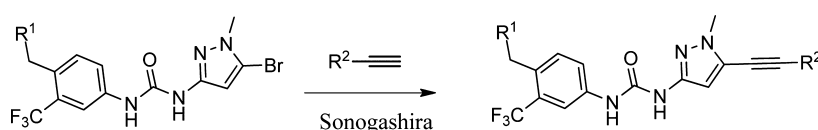


Figure 8. Example of Sonogashira coupling chemistry used in the automated synthesis of Abl inhibitors.

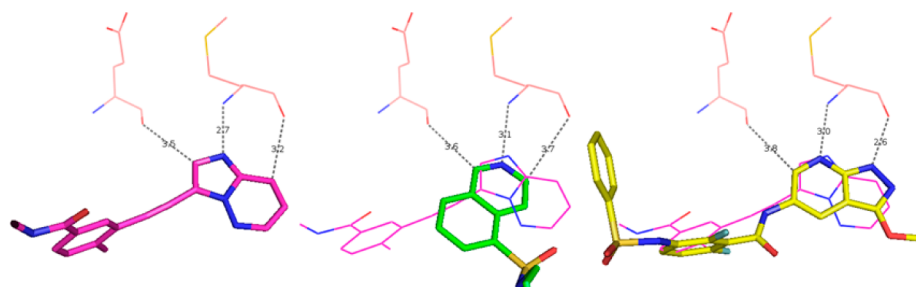


Figure 9. Examples of heterocycles that mimic the R^2 moiety of ponatinib in terms of the attachment vector and the interactions with E316 (top left) and M318 (top right). The commonly observed hinge-binding donor-acceptor-donor functionality can be achieved from the same ring (PDB entry 1YDR, green) or by alternative ring systems (3SKC, yellow).

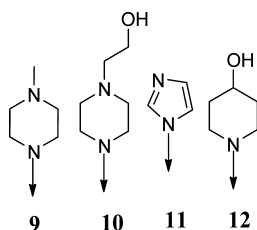


Figure 10. Selected R^1 substituents for the DFG binding templates.

Synthesis of Novel R^2 Alkynes. Noncommercial aromatic alkynes were synthesized from their precursor aromatic bromide or iodide using standard methodology as shown in Scheme 4.

The halo-aromatic or halo-heteroaromatic substrate was treated with ethynyltrimethylsilane **20** under palladium and copper-catalyzed Sonogashira conditions to yield the trimethylsilyl protected alkynes **21**. The TMS group was easily removed using potassium carbonate to yield the free alkynes **22**. The commercial and synthesized alkynes used on the platform as hinge binding motifs are shown in Table 2.

The combination of the 10 DFG binding templates and 27 hinge binding motifs defines the set of 270 compounds available for immediate synthesis on the platform.

Sonogashira Flow Chemistry Methods. Compounds selected by the design algorithm were synthesized on the platform by employing Sonogashira reactions in flow using a Vaportec R4 synthesizer (Figure 11) remotely controlled from a central computer and using a linked modified Gilson 215 sample handler to automatically load injection loops. A 1 mm ID copper coil heated at 150 °C was used as a flow reactor, and the two selected solutions in DMF containing either template or alkyne and palladium catalyst, both at 120 mM concentration of reactant, were mixed and passed through the coil at a total flow rate of 100 μ L/min to give a total reaction time of 20 min. The outflow was filtered through 250 mg of silica contained in a 5 mL 0.6 cm ID Omnifit glass tube to remove metal catalysts and then passed to a 10 μ L injection loop switched automatically at the point of maximum product concentration and thence to the integrated LC/MS purification and bioassay system.

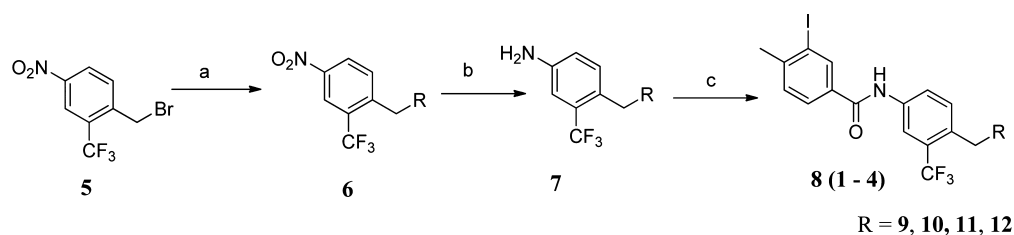
2.3. Algorithm Driven Design Strategies. A key feature of the technology is the employment of computational activity prediction methodology coupled with automated synthesis of compounds (from the virtual chemical space) according to a chosen design strategy. This utilizes Random Forest activity prediction employing one or both of two design strategies — “chase potency” and “most active under sampled”.

Table 1. Synthesised DFG Binding Templates of Types A, B, and C

8-1 ^a	8-2 ^a	8-3 ^a	8-4 ^a
8-5	16-1 ^b	16-2 ^b	
16-3 ^b	16-4 ^b	19 ^c	

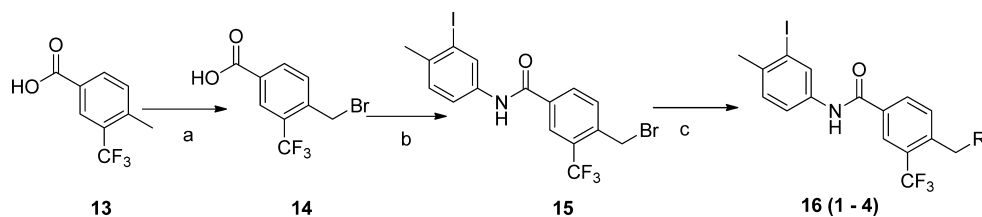
^aType A, Synthesis Scheme 1. ^bType B, Synthesis Scheme 2. ^cType C, Synthesis Scheme 3.

Scheme 1. Synthesis of Ponatinib Templates A^a



^aReagents and conditions: (a) R = piperazine, 4-hydroxyethylpiperazine, imidazole, 4-hydroxypiperidine, CH₂Cl₂, 1 h, (b) H-Cube Hydrogenation, 40 °C, 10% Ra-Ni CatCart (THS01112), MeOH, (c) 3-iodo-4-methylbenzoyl chloride, cat. DMAP, (*i*-Pr)₂NEt, THF, RT.

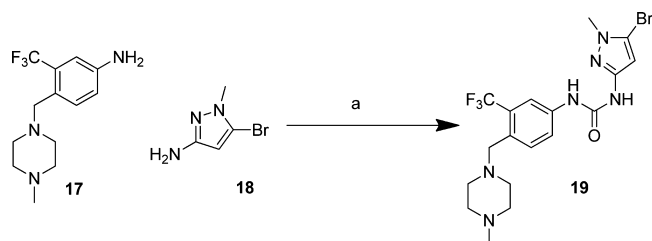
Scheme 2. Synthesis of Reversed Amide Templates B^a



^aReagents and conditions: (a) NaBrO₃, NaSO₃H, EtOAc/H₂O, 50 °C 18 h. (b) 1-Chloro-*N,N*,2-trimethyl-1-propenylamine, Et₃N, (c) 9, 10, 11, or 12, CH₂Cl₂, 1 h.

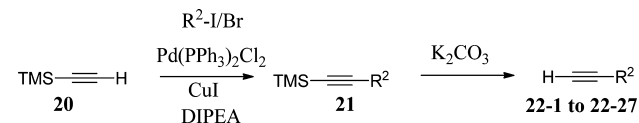
Random Forest Activity Prediction. Regression models are built using the Random Forest method implemented in R accessed via the Pipeline Pilot 'Learn R Forest Model' component.⁴³ The default settings of this component are used except for the molecular descriptors: ALogP, Molecular _

Weight, Num_H_Donors, Num_H_Acceptors, Num_RotatableBonds, Molecular_SurfaceArea, Molecular_PolarSurfaceArea, which are used together with ECFP₆ fingerprints. The fingerprints are not folded and are used as an array of counts. The Random Forest algorithm was chosen because it can

Scheme 3. Synthesis of Pyrazole Urea Template C^a

^aReagents and conditions: (a) 17, CDI, DMSO, rt, 30 min, 18 1 h.

Scheme 4. Synthesis of Aromatic Alkynes from Aryl Halides



perform nonlinear regression, is resistant to overfitting, and has very few tuning parameters.⁴⁴ In all cases the dependent variable is pIC_{50} . Activity values for which only an upper or lower bound is known are treated as follows: lower bound values like ' $IC_{50} < \text{value}$ ' are considered the same as ' $IC_{50} = \text{value}$ '. Upper bound values like ' $IC_{50} > \text{value}$ ' are interpreted as 'inactive'. The user can supply a detection limit for IC_{50} values which will substitute 'inactive' values. If this value is not supplied, compounds with 'inactive' values are ignored. Since the system is designed to run unsupervised, the training set is not split to derive model performance metrics like the R^2 correlation coefficient.

Design Strategies. (a) *Chase Potency.* The activity is predicted for all members of the pool of eligible virtual compounds. The compounds are sorted high to low by predicted activity, and the top scoring compound(s) are selected for synthesis.

(b) *Most Active Under Sampled.* This is a variant on the Latin Hypercube Design.⁴⁵ For each reactant, the number of times it has been incorporated into a previously selected product is counted. Only attempted syntheses carried out during the current experiment are included; i.e., the number of times a reactant has been used to synthesize a prior knowledge compound does not count. For each eligible virtual product, the total is calculated of the number of times the constituting reactants have been used previously. The compounds with the lowest total previous usage are considered to be under sampled, and synthesizing compounds from this pool ensures all reactants are sampled as equally as possible. This is assumed to accelerate learning and coverage of the chemical space although diversity of the products is not explicitly taken into account, and more advanced reagent selection algorithms^{46–49} may be needed if increasing and optimal sampling of product diversity is considered paramount. Typically more compounds are present in the group of under sampled compounds than are desired for the next round of synthesis; therefore this group is further ranked by the "chase potency" strategy to pick the most promising compound(s).

Combined Strategy. It is also possible to operate the platform using a combined strategy that automatically switches between "chase potency" and "most active under sampled" methods, sequentially running multiple loops of each type as defined by the operator.

Prior Knowledge Compounds. Construction of the activity prediction model requires knowledge of activity of compounds from within the virtual chemical space or in similar external chemical space. This may be available from HTS data, the literature, or by off-line synthesis and screening of analogues. Fortunately, the Abl1 IC_{50} activity of numerous ponatinib analogues has been published,²⁶ so a total of 36 literature compounds were used to seed the design model in this work. The full prior knowledge data set is provided in Supporting Information, Table S1. The heat map of predicted activity of the set of 270 compounds available for synthesis on the platform, based on seeding the model with this prior knowledge set, is shown in Figure 12.

2.4. Platform Validation. Prior to commencing SAR generation on the microfluidic platform validation tests were run to ensure platform IC_{50} data were consistent, both with a manual assay and literature data. Imatinib was chosen as a suitable Abl1 inhibitor and was synthesized in flow⁵⁰ and screened against Abl1 both on the platform and manually off-line. The Abl1 activity values derived from the platform are consistent with the manual assay and literature values (Table 3). Experimental details are provided in Supporting Information.

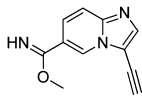
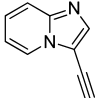
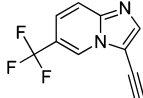
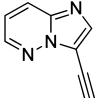
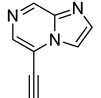
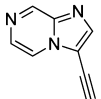
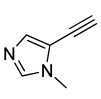
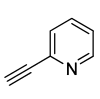
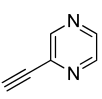
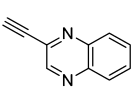
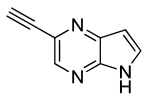
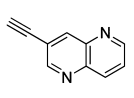
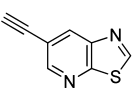
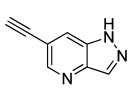
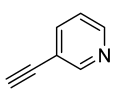
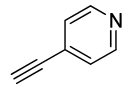
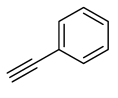
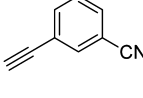
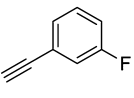
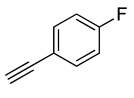
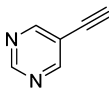
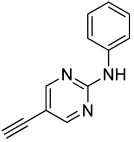
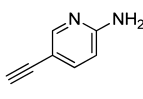
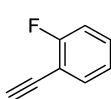
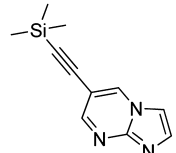
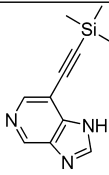
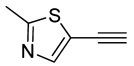
2.5. Experimental Strategy. To fully explore SAR using the design–synthesis–screen methodology, the experimentation on the microfluidic platform was split into three parts. In part one the "most active under sampled" design strategy was used to maximize coverage of the design space and rapidly identify areas of higher activity; in part two the "chase potency" strategy was applied to further map the high activity areas; and finally in part three the "combined" strategy was used to identify and optimize additional potential activity "hot spots".

3. RESULTS AND CONCLUSIONS

Platform SAR Generation - Part One. Once the Abl1 and Abl2 biochemical assays, synthetic protocols, and reactants were in place on the platform, the first round of design–synthesis–screening loops was initiated using the "most active under sampled" methodology in order to accelerate the learning of the activity algorithm and quickly provide an SAR landscape across the virtual chemical space. The first fully automated experiment consisted of 29 loops yielding SAR for 22 new compounds, with 6 compounds failing synthesis and one failing assay quality control (QC) (76% success rate). Each design–synthesis–screening loop took 90 min to complete with a total instrument time of approximately 30 h. It quickly delivered an SAR heat map (Figure 13) that identified "hot-spots" of activity, along with areas of weak potency.

In particular, the pyrazole urea template (19) was rapidly identified as having exciting levels of Abl1 and Abl2 enzyme inhibition, with the 7th, 10th and 16th analogues to be made containing this motif. The ponatinib template 8-1 showed excellent levels of Abl1 and Abl2 potency and gave the most potent compound (synthesized in loop 26) in combination with a novel hinge-binding heterocycle (from alkyne 22-5). Novel templates from the ponatinib series A, e.g., 8-2 used in loop 27 also showed reasonable Abl1 potency ($IC_{50} = 60$ nM). As stated above, a number of phenyl motifs were purposely included that would not be expected to form interactions at the hinge and therefore would be weak Abl inhibitors. This was rapidly confirmed within this part of the experiment, for example, the 4-fluorophenyl motif 22-20 combined with the reverse amide template 16-1 in loop 17 had an Abl1 IC_{50} of

Table 2. Synthesized and Commercial Hinge Binding Aromatic Alkynes Used on the Platform

				
22-1	22-2*	22-3	22-4	22-5
				
22-6	22-7*	22-8*	22-9*	22-10
				
22-11	22-12	22-13	22-14*	22-15*
				
22-16*	22-17*	22-18*	22-19*	22-20*
				
22-21*	22-22*	22-23*	22-24*	22-25 ^a
				
22-26 ^a	22-27			

^aCompound stored with the TMS group present to assist stability. This was removed during platform synthesis. *Commercially available compounds.

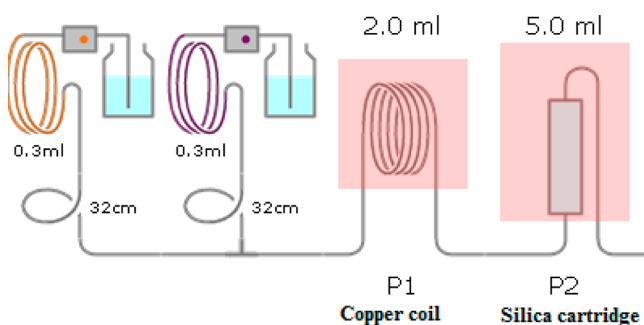


Figure 11. Schematic of the flow apparatus used in the Sonogashira flow synthesis.

only 1.5 μ M. The compounds synthesized in loops 19, 23, and 24 also showed this trend, enabling the model to correctly predict weak activity for all the phenyl motifs.

Platform SAR Generation - Part Two. A second experiment was carried out applying the “chase potency” paradigm, looking to optimize potency within the active areas identified in part one. The experiment consisted of 20 design-loops, yielding 14 additional compounds (6 compounds failed in synthesis, 70% success rate) and delivered a refined heat map (Figure 14). The novel hinge-binding heterocycle (from alkyne 22-5) gave potent activity in the pyrazole urea (loop 30), amide (loop 33), and reverse amide (loop 36) templates, confirming the activity first seen in loop 26. As well as identifying these areas of high activity, the model also predicted activity in the areas associated with, for example, motifs 22-14, 22-25, and 22-26.

Platform SAR Generation - Part Three. A final experiment was carried out using the “Combined” design strategy, by repeatedly applying six loops of “most active under sampled” followed by six loops of “chase potency”. The

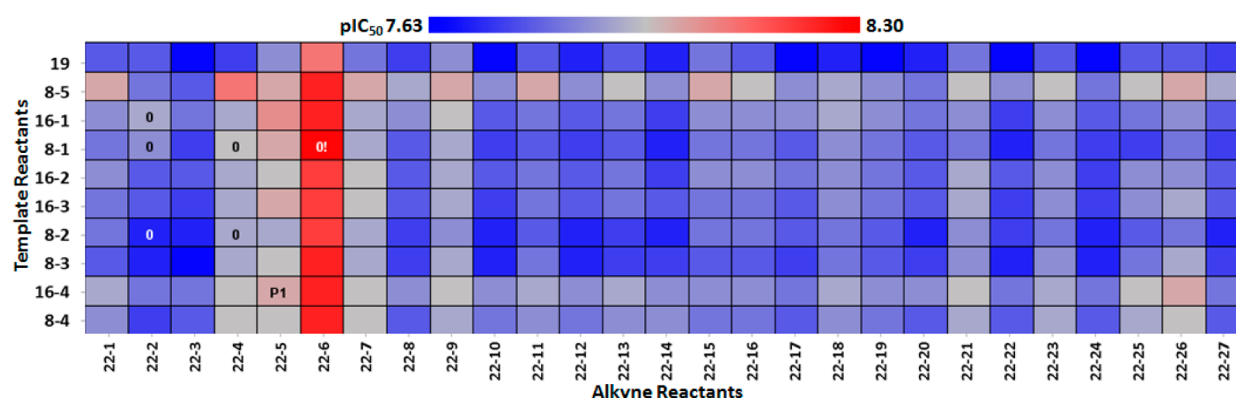
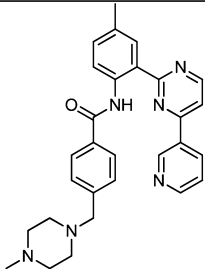


Figure 12. Initial heat map of predicted Abl1 activities of the 270 potential inhibitors based on the prior knowledge data. Prior knowledge compounds are labeled '0', the most active compound found so far by 'P1' and the virtual compound selected for synthesis by 'P1' (the 'most active under sampled' strategy was applied precluding selection from column 22-6).

Table 3. Platform Validation Data

Compound	Structure	Abl1 IC ₅₀ (nM)		
		Platform Assay ^a	Manual Assay ^a	Literature ^b
Imatinib 1		319	190	250

^aAverage of two independent experiments. ^bReference 51.

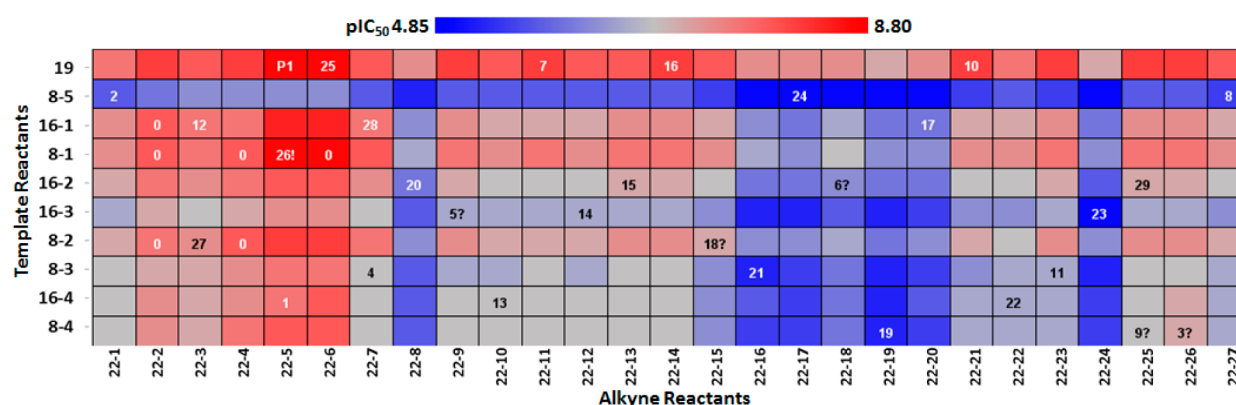


Figure 13. Heat map of predicted Abl1 activities after 29 design-synthesis-screening loops using the "most active under sampled" strategy. Numbers within the heat map indicate order of synthesis with prior knowledge compounds assigned '0'. The most active compound found so far is labeled with '!' and '?' indicates a synthesis, QC, or bioassay failure.

experiment consisted of 41 design-loops, yielding 28 additional compounds (13 compounds failed in synthesis, 68% success rate) and delivered the final activity heat map (Figure 15). The chemical space explored more thoroughly in this part included the areas predicted to have activity at the end of part 2, in particular, the compounds derived from hinge binders 22-25 and 22-26.

In total, 90 design-synthesis-screening loops provided 64 new compounds with a measured IC₅₀ against Abl1 and Abl2. Overall the flow chemistry, purification, and bioassay proceeded with a success rate of 71%. It is worthy of note that the microfluidic platform is able to screen and identify active compounds even when the chemistry is low yielding; for example, in loop 44 the chemical yield was only 8%, but a 3 nM

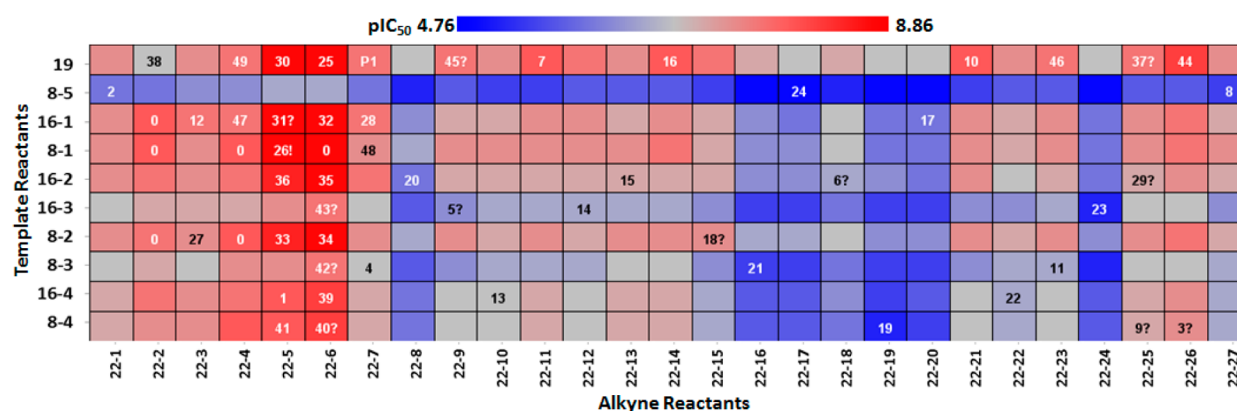


Figure 14. Heat map of predicted Abl1 activities after 49 design–synthesis–screening loops. Numbers within the heat map indicate order of synthesis with prior knowledge compounds assigned '0'. The most active compound found so far is labeled with '!' and '?' indicates a synthesis, QC, or bioassay failure.

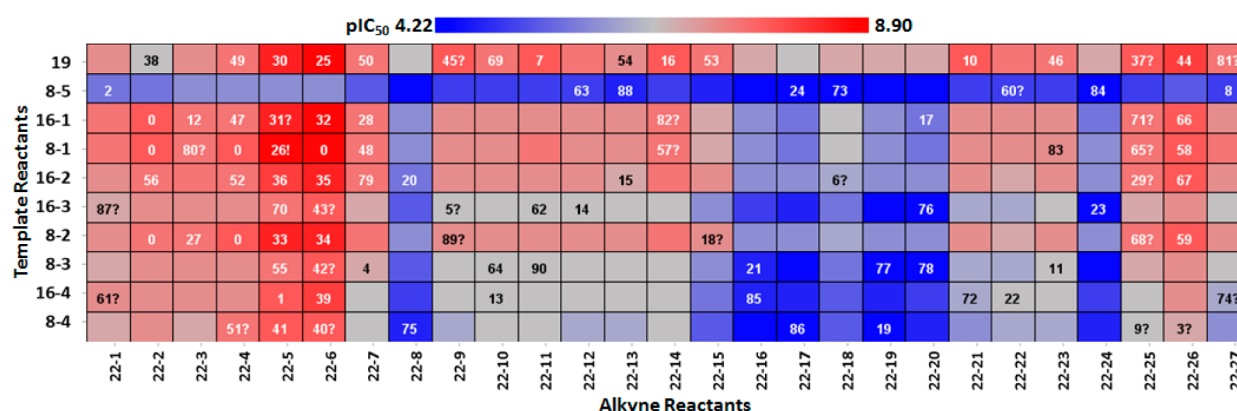


Figure 15. Heat map of predicted Abl1 activities after 90 design–synthesis–screening loops. Numbers within the heat map indicate order of synthesis with prior knowledge compounds assigned '0'. The most active compound found so far is labeled with '!' and '?' indicates a synthesis, QC, or bioassay failure.

Abl1 inhibitor was nominally identified. This attribute is associated with the excellent resolution of byproducts from the desired compound during HPLC purification, combined with microfluidic integration and minimized manipulation of material between synthesis and screening. Full SAR and analytical data from the 90 design-synthesis-screening loops may be found in the Supporting Information, Table S2.

SAR Follow-up. To cross-compare kinase inhibition data generated on the microfluidic platform with that of a solid sample, a number of key compounds were resynthesized (Table 4). These included compounds **23**, **25**, and **26** from the novel pyrazole-urea series, along with compound **24** from the amide series containing a novel hinge-binding heterocycle. This was combined with a group of moderately potent (20–50 nM) and weaker examples (>100 nM). In general, repeat data generated on solid samples were in good agreement with data generated via the microfluidic platform. Two exceptions were the pyrimidine hinge-binder **27** that appeared to be Abl1 selective on the platform but was confirmed as a weak and nonselective compound on retest. Another exception was the pyrazole urea **28**, which was predicted to be moderately active but was weak when synthesized and screened on the platform. Retest of a fresh sample indicated this was a relatively potent Abl inhibitor.

Compounds **23**, **24**, **25**, and **26** were profiled against a number of clinically relevant Abl1 kinase mutants, including H396P, M351T, Q252H, T315I, and Y253F (Table 5). This

confirmed that the novel pyrazole urea Abl template retained potent activity against all clinically relevant Abl1 mutants. In addition, P38 α /MAPK14 data were generated, as the pyrazole unit was identified from vectors observed in pyrazole ureas from P38 inhibitors. Gratifyingly, pyrazole ureas **23**, **25**, and **26** and the novel hinge-binder **24** were all selective for Abl1 over P38 α .⁵³

Compounds **23**–**26** were also screened in human liver microsomal and cell permeability assays, to assess the broader ADME properties of this series (Table 6).⁵⁴

While membrane permeability for the ureas **23**, **25**, and **26** is reduced when compared with amide **24**, this is not entirely unexpected due to the polar and solvated nature of ureas. Compound **26** possessed the best membrane permeability of the ureas, and this was also combined with the lowest *in vitro* clearance in human liver microsomes. Further design and optimization loops could subsequently look to address the reduced permeability of the pyrazole ureas.

In summary, this program details a novel paradigm in hit-to-lead and lead optimization. After the initial design of a virtual chemical space and brief optimization of synthesis and screening, a series of microfluidic synthesis-screening loops were carried out in ~90 min for each iteration. Incorporation of each data point into the choice of subsequent analogue synthesis and deliberately sampling across the virtual chemical space resulted in a heat map visually remarkably similar to the

Table 4. Key Compound IC₅₀ Data

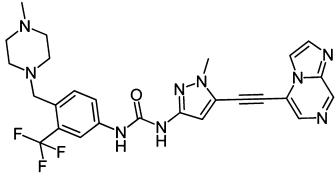
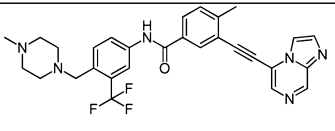
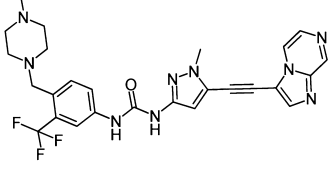
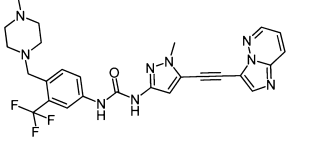
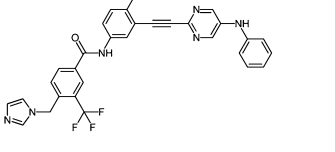
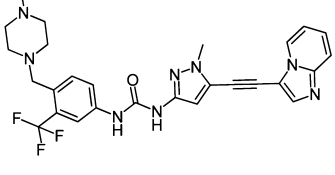
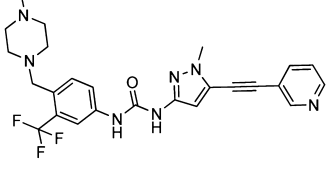
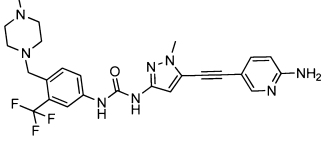
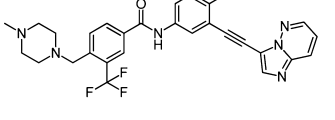
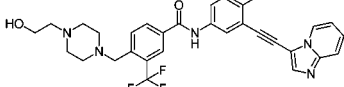
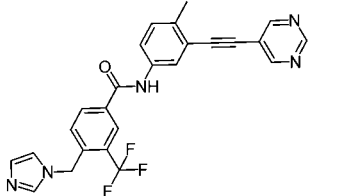
Compound number	Structure	Predicted ^a Abl1 IC ₅₀ (nM)	Platform ^b Abl1 / Abl2 IC ₅₀ (nM)	Retest ^c Abl1 / Abl2 IC ₅₀ (nM)
23		3	2 / 11	12 / 15
24		2	0.2 / 2	1 / 1
27		1	0.4 / 3	7 / 10
26		30	27 / 47	12 / 6
27		400	234 / >10,000	307 / 298
28		200	3000, >10,000	30 / 12
29		30	33 / 66	31 / 14
30		30	42 / 67	22 / 36
31 ^d		20	45 / 39	15 / 8

Table 4. continued

Compound number	Structure	Predicted ^a Abl1 IC ₅₀ (nM)	Platform ^b Abl1 / Abl2 IC ₅₀ (nM)	Retest ^c Abl1 / Abl2 IC ₅₀ (nM)
32		20	27 / 41	13 / 18
33		500	228 / 163	40 / 40

^aPrediction after 90 synthesis to screening loops. ^bReplicates $n = 1$. ^cReplicates $n = 4$. ^dPreviously reported.⁵²

Table 5. Activity of Resynthesized Compounds vs. WT and Mutant Abl Kinases and P38 α

	IC ₅₀ (nM) ^a			
	23	24	25	26
Abl1 WT	1.6	0.6	1.0	1.0
H396P	0.7	0.3	0.3	0.2
M351T	0.9	0.3	0.5	0.4
Q252H	1.6	0.5	1.0	0.7
T315I	1.9	0.4	0.8	0.4
Y253F	0.9	0.3	0.4	0.4
P38 α /MAPK14	35	43	35	24

^aReplicates $n = 1$.

Table 6. Data from Human Liver Microsomal and Cell Permeability Assays

compound	23	24	25	26
HLM CL _{int} ^a (μ L/min/mg protein)	76	90	51	29
PAMPA ^b Papp (10^{-6} cm ⁻¹)	0.1	26	0.2	2

^aReplicates $n = 5$. ^bReplicates: 23 and 24, $n = 3$; 25, $n = 2$; 26, $n = 4$.

one at the end of the experiment for 270 compounds with only 22 compounds synthesized and quickly identified the pyrazole-urea DFG-out motif as an unprecedented replacement for the benzamide present in ponatinib. Further loops of design-synthesis-screening refined the heat map and led to the discovery of compounds 23, 24, 25, and 26, as novel and potent Abl1 and Abl2 inhibitors. Further off-line screening demonstrated that 23, 24, 25, and 26 possessed potent Abl mutant activity, including the key T315I gatekeeper mutant.

Microfluidic synthesis, purification, and screening show great potential for reducing the time required for the design-synthesis-test loop at the core of preclinical drug discovery. When this technology is combined with an activity prediction algorithm and appropriate automated design strategies, the technology platform can deliver extremely rapid optimization of compound series and an accurate SAR heat map for the series.

4. EXPERIMENTAL SECTION

Chemistry. General Introductory Section. Identification, quantitation (assay sample concentration and chemical yield are determined using a calibrated evaporative light scattering detector (ELSD)), and selection of compounds synthesized on the platform were performed by analytical LC-MS-UV-ELSD analysis. This was conducted using the following instrument and conditions. Waters Acquity BSD pump, PolymerLabs 2100-ICE 385 ELS detector and Waters Acquity PDA set at 254 nm with the MS detection performed on a Waters SQ mass spectrometer with atmospheric pressure chemical ionization (APCI); Phenomenex Luna 5 μ m C18(2) 100 Å 150 \times 4.6 mm column; solvent A, water–0.1% formic acid; solvent B, acetonitrile–0.1% formic acid; flow rate 1.5 mL/min; start 10% B with 0.2 min initial hold, final 99% B in 8.8 min, linear gradient. Purity determination for selected samples was performed using analytical high performance liquid chromatography (HPLC) with the following instrument and conditions. Gilson 322 pump, 155 detector, 819 injector, and Agilent 385 ELS detector; Phenomenex Gemini 5 μ m C18 110 Å 100 \times 4.6 mm column; solvent A, 20 mM ammonium acetate in water pH 7; solvent B, acetonitrile; flow rate 1.5 mL/min; start 2% B, final 98% B in 8 min, linear gradient. Compounds purified by reverse-phase high performance liquid chromatography (RP-HPLC) used the following instrument and conditions. Gilson 322 pump, 155 detector, 819 injector, and FC204 fraction collector; Phenomenex Luna 5 μ m C18(2) 100 Å, AXIA Packed, 150 \times 21.2 mm column; solvent A, water–0.5% formic acid; solvent B, acetonitrile–0.5% formic acid; flow rate 18 mL/min; start 10 to 40% B, final 50 to 98% B in 7 min, linear gradient. Starting and final percentage of solvent B were on a per compound basis. All microwave reactions were carried out in the Biotage Initiator Sixty microwave reactor. NMR measurements were performed on an Oxford Instruments 400 MHz NMR instrument using CDCl₃, CD₃OD or DMSO-*d*₆ as solvent. Chemical shifts are reported in ppm and coupling constants (*J*) in Hz. Chemical shifts are reported using solvent as internal standard. Final compounds for biological assay were >95% purity as judged by HPLC and LC-MS analysis as described above.

Synthetic methods and analytical data for noncommercial compounds in Tables 1, 2, and 3 are included in the Supporting Information.

Experimental Section. General Experimental Procedure for Sonogashira Couplings in Batch. To a 10 mL microwave reactor tube fitted with a stirrer bar was added iodide (0.116 mmol), *N*-ethyl-*N*-isopropylpropan-2-amine (0.081 mL, 0.464 mmol), alkyne (0.116 mmol), and DMF (4 mL). Nitrogen was bubbled through the mixture for 2 min and *tetrakis*(triphenylphosphine)palladium(0) (3.35 mg,

2.90 μmol) and copper(I) iodide (0.828 mg, 4.35 μmol) were added. The tube was sealed and heated to 100 $^{\circ}\text{C}$ in microwave for 45 min. The resultant mixture was partitioned between dichloromethane (50 mL) and water (50 mL), the organics were dried (MgSO_4) and filtered, and the solvent was removed by evaporation to give a dark brown residue. The residue was purified by preparative HPLC.

Analytical Data for Compounds in Table 4. 1-(5-(Imidazo[1,2-*a*]pyrazin-5-ylethynyl)-1-methyl-1*H*-pyrazol-3-yl)-3-(4-((4-methylpiperazin-1-yl)methyl)-3-(trifluoromethyl)phenyl)urea (**23**) (5%). ^1H NMR ($\text{DMSO}-d_6$): δ 9.4 (d, J = 12, 2H), 9.36 (s, 1H), 8.7 (d, J = 4, 1H), 8.1 (d, J = 4, 1H), 7.96 (s, 1H), 7.6 (m, 1H), 6.7 (s, 1H), 3.8 (s, 3H), 3.5 (s, 2H), 2.53 (m, 8H), 2.13 (s, 3H). ^{13}C NMR ($\text{DMSO}-d_6$): δ 28.54, 37.57, 46.15, 53.62, 55.17, 55.83, 82.47, 88.44, 100.72, 100.08, 119.80, 122.03, 124.37, 130.55, 131.28, 131.80, 139.16, 140.61, 147.18, 152.29.

MS: m/z 538.5 $[\text{M} + \text{H}]^+$

3-(Imidazo[1,2-*a*]pyrazin-5-ylethynyl)-4-methyl-*N*-(4-((4-methylpiperazin-1-yl)methyl)-3-(trifluoromethyl)phenyl)benzamide (**24**) (31%). ^1H NMR ($\text{DMSO}-d_6$): δ 10.53 (s, 1H), 9.19 (s, 1H), 8.65 (d, J = 4, 1H), 8.27 (m, 1H), 8.25 (s, 1H), 8.19 (m, 1H), 8.12 (d, J = 4, 1H), 8.03–8.06 (m, 1H), 7.93–7.95 (m, 1H), 7.68 (d, J = 8, 1H), 7.53 (d, J = 8, 1H), 3.15 (s, 2H), 2.60 (s, 3H), 2.37 (br, 8H), 2.16 (s, 3H). ^{13}C NMR ($\text{DMSO}-d_6$): δ 165.09, 143.88, 143.70, 138.58, 131.28, 129.09, 123.94, 121.86, 119.46, 119.45, 117.65, 98.39, 80.25, 57.87, 57.85, 55.11, 53.03, 46.05, 22.95, 21.02.

MS: m/z 533 $[\text{M} + \text{H}]^+$

1-(5-(Imidazo[1,2-*a*]pyrazin-3-ylethynyl)-1-methyl-1*H*-pyrazol-3-yl)-3-(4-((4-methylpiperazin-1-yl)methyl)-3-(trifluoromethyl)phenyl)urea-formate salt (**25**) (5.2%). ^1H NMR ($\text{DMSO}-d_6$): δ 9.4 (s, 1H), 9.32 (s, 1H), 9.2 (s, 1H), 8.7 (d, 1H), 8.28 (d, 1H), 8.1 (s, 1H), 7.6 (t, 1H), 6.71 (s, 1H), 3.88 (s, 3H), 2.39 (m, 8H), 2.21 (s, 3H). ^{13}C NMR ($\text{DMSO}-d_6$): δ 37.57, 45.61, 52.62, 54.26, 54.86, 57.10, 84.63, 87.92, 100.72, 109.98, 115.41, 122.03, 124.39, 126.16, 127.86, 130.39, 131.29, 131.86, 139.20, 140.63, 143.69, 147.10, 152.36.

MS: m/z 538.5 $[\text{M} + \text{H}]^+$

1-(5-(Imidazo[1,2-*b*]pyridazin-3-ylethynyl)-1-methyl-1*H*-pyrazol-3-yl)-3-(4-((4-methylpiperazin-1-yl)methyl)-3-(trifluoromethyl)phenyl)urea-formate salt (**26**) (20.6%). ^1H NMR ($\text{DMSO}-d_6$): δ 9.37 (d, J = 4, 2H), 8.7 (d, J = 4, 1H), 8.25 (s, 2H), 7.93 (s, 1H), 7.6 (s, 2H), 7.4 (dd, J = 8, 4, 1H), 6.66 (s, 1H), 3.86 (s, 3H), 3.5 (s, 2H), 2.3 (m, 8H), 2.2 (s, 3H). ^{13}C NMR ($\text{DMSO}-d_6$): δ 37.32, 45.08, 52.14, 54.56, 57.58, 83.79, 86.49, 100.07, 111.37, 115.4, 119.85, 123.41, 126.14, 127.88, 130.26, 139.25, 140.33, 145.59, 152.27, 152.36, 164.24.

MS: m/z 538 $[\text{M} + \text{H}]^+$

4-((1*H*-Imidazol-1-yl)methyl)-*N*-(4-methyl-3-((5-(phenylamino)pyrimidin-2-yl)ethynyl)phenyl)-3-(trifluoromethyl)benzamide (**27**) (6.45%). ^1H NMR (CDCl_3): δ 8.50 (s, 2H), 8.40 (m, 1H), 8.15 (m, 1H), 8.0 (s, 1H), 7.85 (m, 1H), 7.65 (m, 3H), 7.55 (m, 1H), 7.25–7.35 (m, 6H), 7.1 (s, 1H), 7.0 (m, 1H), 5.6 (s, 2H), 2.4 (s, 3H).

MS: m/z 553 $[\text{M} + \text{H}]^+$

1-(5-(Imidazo[1,2-*a*]pyridin-3-ylethynyl)-1-methyl-1*H*-pyrazol-3-yl)-3-(4-((4-methylpiperazin-1-yl)methyl)-3-(trifluoromethyl)phenyl)urea-formate salt (**28**) (16%). ^1H NMR ($\text{DMSO}-d_6$): δ 9.34 (d, J = 8, 1H), 8.6 (d, J = 8, 1H), 8.1 (s, 1H), 8.06 (s, 1H), 7.95 (s, 1H), 7.74 (d, 1H), 7.58 (m, 2H), 7.45 (m, 1H), 7.14 (m, 1H), 6.6 (s, 1H), 3.8 (s, 3H), 3.5 (s, 2H), 2.48 (m, 8H), 2.30 (s, 3H).

MS: m/z 537.5 $[\text{M} + \text{H}]^+$

1-(1-Methyl-5-(pyridin-3-ylethynyl)-1*H*-pyrazol-3-yl)-3-(4-((4-methylpiperazin-1-yl)methyl)-3-(trifluoromethyl)phenyl)urea-formate salt (**29**) (8%). ^1H NMR ($\text{DMSO}-d_6$): δ 9.21 (d, J = 8, 1H), 9.14 (d, J = 8, 1H), 8.8 (s, 1H), 8.6 (d, J = 4, 1H), 8.15 (s, 1H), 8.05 (d, J = 7.5, 1H), 7.58 (m, 1H), 7.49 (dd, J = 8, 4, 1H), 6.62 (s, 1H), 3.85 (s, 3H), 3.5 (s, 2H), 2.3 (m, 8H), 2.15 (s, 3H).

MS: m/z 498.5 $[\text{M} + \text{H}]^+$

1-(5-(6-Aminopyridin-3-yl)ethynyl)-1-methyl-1*H*-pyrazol-3-yl)-3-(4-((4-methylpiperazin-1-yl)methyl)-3-(trifluoromethyl)phenyl)urea-formate salt (**30**) (5%). ^1H NMR ($\text{DMSO}-d_6$): δ 9.1 (s, 1H), 8.15 (m, 1H), 7.91 (m, 1H), 7.55 (m, 2H), 6.44 (m, 2H), 3.80 (s, 3H), 3.5 (s, 2H), 2.3 (m, 8H), 2.2 (s, 3H) (5%).

MS: m/z : 513.5 $[\text{M} + \text{H}]^+$

4-((4-(2-Hydroxyethyl)piperazin-1-yl)methyl)-*N*-(3-(imidazo[1,2-*a*]pyridin-3-ylethynyl)-4-methylphenyl)-3-(trifluoromethyl)benzamide (**32**) (25%). ^1H NMR (CDCl_3): δ 8.35 (d, J = 8, 1H), 8.24 (s, 1H), 8.15 (s, 2H), 8.04 (d, J = 8, 1H), 7.91 (m, 2H), 7.90 (s, 1H), 7.65 (d, J = 12, 1H), 7.53 (dd, J = 4, 8, 1H), 7.29 (m, 2H), 6.96 (t, J = 4, 1H), 3.74 (s, 1H), 3.67 (t, J = 4, 2H), 2.65 (br m, 8H), 2.60 (br m, 3H), 2.54 (s, 2H).

MS: m/z 562 $[\text{M} + \text{H}]^+$

4-((1*H*-Imidazol-1-yl)methyl)-*N*-(4-methyl-3-(pyrimidin-5-ylethynyl)phenyl)-3-(trifluoromethyl)benzamide (**33**) (8.49%). ^1H NMR ($\text{DMSO}-d_6$): δ 10.5 (s, 1H), 9.18 (s, 1H), 9.08 (s, 2H), 8.31 (s, 1H), 8.18 (d, J = 8, 1H), 8.02 (d, J = 4, 1H), 7.78 (s, 1H), 7.67 (dd, J = 8, 8, 1H), 7.33 (d, J = 8, 1H), 7.19 (s, 1H), 7.08 (d, J = 8, 1H), 6.98 (s, 1H), 3.15 (s, 2H), 2.45 (s, 3H).

MS: m/z 462 $[\text{M} + \text{H}]^+$

(a) **Biology Platform Kinase Assays:** The Omnia kinase activity assay technology was employed to monitor real-time kinase activity on the platform. Full details are provided in Supporting Information.

■ ASSOCIATED CONTENT

● Supporting Information

Detailed synthetic chemistry data, detailed biological methods, prior knowledge data table, full SAR derived using the automated platform. This material is available free of charge via the Internet at <http://pubs.acs.org>.

■ AUTHOR INFORMATION

Corresponding Author

*E-mail: chris.selway@cyclofluidic.co.uk. E-mail: +44 (0)1707 358674.

Author Contributions

The manuscript was written through contributions of all authors.

Notes

The authors declare the following competing financial interest(s): Sandexis LLP act as medicinal and computational chemistry consultants to Cyclofluidic Ltd; and Accelrys Ltd provide consulting services to Cyclofluidic Ltd.

■ ACKNOWLEDGMENTS

We would like to thank Pfizer, UCB and Accelrys for their technical support and advice, and Heptares Therapeutics is duly acknowledged for the generous loan of their H-Cube Hydrogenation Reactor. Funding is by Pfizer Ltd., Ramsgate Road, Sandwich, Kent, CT13 9NJ, U.K. UCB Pharma, 208 Bath Road, Slough, Berkshire SL1 3WE, UK. UK Technology Strategy Board. The UK Technology Strategy Board is an executive nondepartmental public body (NDPB), established by the Government in 2007 and sponsored by the Department for Business, Innovation and Skills (BIS).

■ ABBREVIATIONS USED

BLAST, Basic Local Alignment Search Tool

■ REFERENCES

- (1) Paul, S. M.; Mytelka, D. S.; Dunwiddie, C. T.; Persinger, C. C.; Munos, B. H.; Lindborg, S. R.; Schacht, A. L. How to improve R&D productivity: the pharmaceutical industry's grand challenge. *Nat. Rev. Drug Discovery* **2010**, *9*, 203–241.
- (2) Kola, I.; Landis, J. Can the pharmaceutical industry reduce attrition rates? *Nat. Rev. Drug Discovery* **2004**, *3*, 711–715.
- (3) Rossi, T.; Braggio, S. Quality by Design in lead optimization: a new strategy to address productivity in drug discovery. *Curr. Opin. Pharmacol.* **2011**, *11*, 515–520.

- (4) Proudfoot, J. R. Drugs, leads, and drug-likeness: an analysis of some recently launched drugs. *Bio. Org. Med. Chem. Lett.* **2002**, *12* (12), 1647–1650.
- (5) Oprea, T. I.; Davis, A. M.; Teague, S. J.; Leeson, P. D. Is There a Difference between Leads and Drugs? A Historical Perspective. *J. Chem. Inf. Comput. Sci.* **2001**, *41*, 1308–1315.
- (6) Clark, D. E.; Pickett, S. D. Computational methods for the prediction of 'drug-likeness'. *Drug Discovery Today* **2000**, *5* (2), 49–58.
- (7) Leeson, P. D.; Springthorpe, B. The influence of drug-like concepts on decision-making in medicinal chemistry. *Nat. Rev. Drug Discovery* **2007**, *6*, 881–890.
- (8) Free, S. M.; Wilson, J. W. A Mathematical Contribution to Structure-Activity Studies. *J. Med. Chem.* **1964**, *7* (4), 395–399.
- (9) Craig, P. N. Structure-activity correlations of antimalarial compounds 1. Free-Wilson analysis of 2-phenylquinoline-4-carbinols. *J. Med. Chem.* **1972**, *15* (2), 144–149.
- (10) Schaper, K.-J. Free-Wilson-Type Analysis of Non-Additive Substituent Effects on THPB Dopamine Receptor Affinity Using Artificial Neural Networks. *Quant. Struct.-Activity Relationships* **1999**, *18* (4), 354–360.
- (11) Wong Hawkes, S. Y. F.; Chapela, M. J. V.; Montembault, M. Leveraging the advantages offered by microfluidics to enhance the drug discovery process. *QSAR Comb. Sci.* **2005**, *24* (6), 712–721.
- (12) Wong-Hawkes, S. Y. F.; Matteo, J. C.; Warrington, B. H.; White, J. D. Microreactors as new tools for drug discovery and development. *Ernst Schering Foundation Symposium Proc.* **2006**, *3*, 39–55.
- (13) Guetzoyan, L.; Nikbin, N.; Baxendale, I. R.; Ley, S. V. Flow chemistry synthesis of zolpidem, alpidem and other GABAA agonists and their biological evaluation through the use of in-line frontal affinity chromatography. *Chem. Sci.* **2013**, *4*, 764–769.
- (14) Ley, S. V.; Baxendale, I. R. The Changing Face of Organic Synthesis. *CHIMIA Int. J. Chem.* **2008**, *62* (3), 162–168.
- (15) Malet-Sanz, L.; Susanne, F. Continuous Flow Synthesis. A Pharma Perspective. *J. Med. Chem.* **2012**, *55* (9), 4062–4098.
- (16) Watts, P. The Application of Microreactors in Combinatorial Chemistry. *QSAR Comb. Sci.* **2005**, *24*, 701–711.
- (17) Glasnov, T. N.; Kappe, C. O. Continuous-flow syntheses of heterocycles. *J. Heterocyclic Chem.* **2011**, *48* (1), 11–30.
- (18) Webb, D.; Jamison, T. F. Continuous flow multi-step organic synthesis. *Chem. Sci.* **2010**, *1*, 675–680.
- (19) Bogdan, A. R.; James, K. Efficient Access to New Chemical Space Through Flow—Construction of Druglike Macrocycles Through Copper-Surface-Catalyzed Azide–Alkyne Cycloaddition Reactions. *Chem. Eur. J.* **2010**, *16*, 14506–14512.
- (20) Lange, P. P.; James, K. Rapid Access to Compound Libraries through Flow Technology: Fully Automated Synthesis of a 3-Aminoindolizine Library via Orthogonal Diversification. *ACS Comb. Sci.* **2012**, *14*, 570–578.
- (21) Druker, B. J.; Alpa, M. T.; Resta, D. J.; Peng, B.; Buchdunger, E.; Ford, J. M.; Lydon, N. B.; Kantajian, H.; Capdeville, R.; Ohno-Jones, S.; Sawyers, C. L. Activity of a Specific Inhibitor of the BCR-ABL Tyrosine Kinase in the Blast Crisis of Chronic Myeloid Leukemia and Acute Lymphoblastic Leukemia with the Philadelphia Chromosome. *N. Engl. J. Med.* **2001**, *344*, 1031–1037.
- (22) Shah, N. P.; Nicoll, J. M.; Nagar, B.; Gorrel, M. E.; Paquette, R. L.; Kuriyan, J.; Sawyers, C. L. Multiple BCR-ABL kinase domain mutations confer polyclonal resistance to the tyrosine kinase inhibitor imatinib (STI571) in chronic phase and blast crisis chronic myeloid leukemia. *Cancer Cell* **2002**, *2* (2), 117–125.
- (23) Kantarjian, H. J.; Giles, F.; Gattermann, N.; Bhalla, K.; Alimena, G.; Palandri, F.; Ossenkoppele, G. J.; Nicolini, F.-E.; O'Brien, S. G.; Litzow, M.; Bhatia, R.; Cervantes, F.; Haque, A.; Shou, Y.; Resta, D. J.; Weitzman, A.; Hochhaus, A.; le Coutre, P. Nilotinib (formerly AMN107), a highly selective BCR-ABL tyrosine kinase inhibitor, is effective in patients with Philadelphia chromosome-positive chronic myelogenous leukemia in chronic phase following imatinib resistance and intolerance. *Blood* **2007**, *110*, 3540–3546.
- (24) Talpaz, M.; Shah, N. P.; Kantarjian, H.; Donato, N.; Nicoll, J.; Paquette, R.; Cortes, J.; O'Brien, S.; Nicaise, C.; Bleickardt, E.; Blackwood-Chirchir, M. A.; Iyer, V.; Chen, T.-T.; Huang, F.; Decillis, A. P.; Sawyers, C. L. Dasatinib in imatinib-resistant Philadelphia chromosome-positive leukemias. *N. Engl. J. Med.* **2006**, *354*, 2531–2541.
- (25) Tanaka, R.; Kimura, S. Abl Tyrosine Kinase Inhibitors for Overriding Bcr-Abl/T3151: From the Second to Third Generation. *Expert Rev. Anticancer Ther.* **2008**, *8*, 1387–1398.
- (26) Huang, W. S.; Metcalf, C. A.; Sundaramoorthi, R.; Wang, Y. Z.; Thomas, R. M.; Zhu, X.; Cai, L.; Wen, D.; Liu, S.; Romero, J.; Qi, J.; Chen, L.; Banda, G.; Lentini, S. P.; Das, S.; Xu, Q.; Keats, J.; Wang, F.; Wardwell, S.; Ning, Y.; Snodgrass, J. T.; Broudy, M. I.; Russian, K.; Zhou, T.; Commodore, L.; Narasimhan, N. I.; Mohemmad, Q. K.; Iulucci, J.; Rivera, V. M.; Dalgarno, D. C.; Sawyer, T. K.; Clackson, T.; Shakespeare, W. C. Discovery of 3-[2-(Imidazo[1,2-b]pyridazin-3-yl)ethynyl]-4-methyl-N-{4-[(4-methylpiperazin-1-yl)methyl]-3-(trifluoromethyl)phenyl}benzamide (AP24534), a Potent, Orally Active Pan-Inhibitor of Breakpoint Cluster Region-Abelson (BCR-ABL) Kinase Including the T315I Gatekeeper Mutant. *J. Med. Chem.* **2010**, *53*, 4701–4719.
- (27) Carlson, R. H. Ponatinib effective in heavily pretreated CML patients with T315I mutation. *Oncology Times UK* **2011**, *8* (3), 17–18.
- (28) <http://www.fda.gov/Drugs/InformationOnDrugs/ApprovedDrugs/ucm332368.htm>
- (29) Lu, X. Y.; Cai, Q.; Ding, K. Recent developments in the third generation inhibitors of Bcr-Abl for overriding T315I mutation. *Curr. Med. Chem.* **2011**, *18*, 2146–2157.
- (30) Shults, M. D.; Imperiali, B. Versatile Fluorescence Probes of Protein Kinase Activity. *J. Am. Chem. Soc.* **2003**, *125*, 14248–14249.
- (31) Kinase assay reagents were purchased from Life Technologies, Paisley, Renfrewshire, UK
- (32) Zhou, T.; Commodore, L.; Huang, W.-S.; Wang, Y.; Thomas, M.; Keats, J.; Xu, Q.; Rivera, V. M.; Shakespeare, W. C.; Clackson, T.; Dalgarno, D. C.; Zhu, X. Structural Mechanism of the Pan-BCR-ABL Inhibitor Ponatinib (AP24534): Lessons for Overcoming Kinase Inhibitor Resistance. *Chem. Biol. Drug Des.* **2011**, *77* (1), 1–11.
- (33) Klüter, S.; Grütter, C.; Naqvi, T.; Rabiller, M.; Simard, J. R.; Pawar, V.; Getlik, M.; Rauh, D. Displacement assay for the detection of stabilizers of inactive kinase conformations. *J. Med. Chem.* **2010**, *53* (1), 357–367.
- (34) Berman, H. M.; Westbrook, J.; Feng, Z.; Gilliland, G.; Bhat, T. N.; Weissig, H.; Shindyalov, I. N.; Bourne, P. E. The Protein Data Bank. *Nucleic Acids Res.* **2000**, *28*, 235–242, www.rcsb.org.
- (35) Deng, X.; Lim, S. M.; Zhang, J.; Gray, N. S. Broad spectrum alkynyl inhibitors of T315I Bcr-Abl. *Bioorg. Med. Chem. Lett.* **2010**, *20*, 4196–4200.
- (36) Zhang, Y.; Jamison, T. F.; Patel, S.; Mainolfi, N. Continuous Flow Coupling and Decarboxylation Reactions Promoted by Copper Tubing. *Org. Lett.* **2011**, *13* (2), 280–283.
- (37) Source for bromoheterocycles search was www.emolecules.com.
- (38) Kearsley, S. J. An algorithm for the simultaneous superposition of a structural series. *J. Comput. Chem.* **1990**, *11*, 1187–1192.
- (39) Ponder, J. W. *Tinker Molecular Modelling Package*; Washington University, St. Louis, MO.
- (40) Shakespeare W. C.; Haluska F. G. WO2012139027, 2012.
- (41) www.thalesnano.com
- (42) Kikuchi, D.; Sakaguchi, S.; Ishii, Y. An Alternative Method for the Selective Bromination of Alkylbenzenes Using NaBrO₃/NaHSO₃ Reagent. *J. Org. Chem.* **1998**, *63* (17), 6023.
- (43) Liaw, A.; Wiener, M. Classification and Regression by Random Forest. *R News* **2002**, *2* (3), 18–22.
- (44) Breiman, L. Random Forests. *Machine Learning* **2001**, *45*, 5–32.
- (45) McKay, M. D.; Conover, W. J.; Beckman, J. R. Comparison of Three Methods for Selecting Values of Input Variables in the Analysis of Output from a Computer Code. *Technometrics* **1979**, *21* (2), 239–245.
- (46) Agrafiotis, D. K. Stochastic Algorithms for Maximizing Molecular Diversity. *J. Chem. Inf. Comput. Sci.* **1997**, *37*, 841–851.

- (47) Agrafiotis, D. K.; Rassokhin, D. N. Design and Prioritization of Plates for High-Throughput Screening. *J. Chem. Inf. Comput. Sci.* **2001**, *41*, 798–805.
- (48) Brown, R. D.; Martin, Y. C. Designing Combinatorial Library Mixtures Using a Genetic Algorithm. *J. Med. Chem.* **1997**, *40*, 2304–2313.
- (49) Gillet, V. J.; Khatib, W.; Willett, P.; Fleming, P. J.; Green, D. V. S. Combinatorial Library Design Using a Multiobjective Genetic Algorithm. *J. Chem. Inf. Comput. Sci.* **2002**, *42*, 375–385.
- (50) Hopkin, M. D.; Baxendale, I. R.; Ley, S. V. An expeditious synthesis of imatinib and analogues utilising flow chemistry methods. *Org. Biomol. Chem.* **2013**, *11*, 1822–1839.
- (51) Capdeville, R.; Buchdunger, E.; Zimmermann, J.; Matter, A. Glivec (STIS71, imatinib), a rationally developed, targeted anticancer drug. *Nat. Rev. Drug Discovery* **2002**, *1*, 493–502.
- (52) Zou, D.; Huang, W. S.; Thomas, R. M.; Romero, J. A. C.; Qi, J.; Wang, Y.; Zhu, X.; Shakespeare, W. C.; Sundaramoorthi, R.; Metcalf, C. A., III; Dalgarno, D. C.; Sawyer, T. K. Bicyclic Heteroaryl Compounds. US Patent Application 2006/048758, December 22, 2006.
- (53) Inhibition assays with ABL1 (H396P), ABL1 (M351T), ABL1 (Q252H), ABL1 (T315I), ABL1 (Y253F), ABL2/ARG and P38 α /MAPK14 were carried out by Reaction Biology Corporation, Malvern, PA, USA.
- (54) In vitro human microsomal stability and parallel artificial membrane permeability assay (PAMPA) assays were carried out by Cypotex Discovery Ltd., Macclesfield, Cheshire, U.K.